Elsevier Editorial System(tm) for Journal of Sound and Vibration

Manuscript Draft

Manuscript Number: JSV-D-19-00373R3

Title: Single-camera single-axis vision method applied to measure vibrations

Article Type: Full Length Article

Section/Category: C Measurement Techniques

Keywords: vibration measurement; vision method; single high-speed camera

Corresponding Author: Dr. Manuel MELON, Ph.D.

Corresponding Author's Institution: Université du Maine

First Author: Thomas DURAND-TEXTE, PhD

Order of Authors: Thomas DURAND-TEXTE, PhD; Manuel MELON, Ph.D.; Elisabeth SIMONETTO, PhD; Stéphane DURAND, PhD; Marie Hélène MOULET

Abstract: Increased interest has been witnessed for full-field techniques measuring vibrations. 3D vision methods coupled to two high-speed cameras have proven to be a valid solution to measure 3D displacements, notably with the Stereo Digital Image Correlation (SDIC) tools. The now conventional pseudo-stereo system with a single high-speed camera and a four-mirror adapter, generating two virtual cameras, may also be used, even if it is rather complex to operate and remains limited to small objects. In a logic of simplification of the protocol, the authors present here a set-up requiring a single high-speed camera and no mirrors, with the associated full-field single-axis vision method. The latter is logically designed to measure the vibrations of items whose displacements are locally along a single axis (usually normal to the surface). This paper reports firstly the results of the full-field measurement of the vibrations of a plate, validated by a comparison with those obtained with the four-mirror adapter set-up, and secondly the application to the full-field measurement of the vibrations of a tambourine. Thirdly, the conventional pseudo-stereo technique and the proposed vision method are compared and assessed, in order to establish their respective limits and potential complementarity. Finally, once the application of the method to plane objects is validated, measurements have been carried out on a non-planar object: a bent plate; the results obtained also validate the proposed approach for non-flat surfaces.

# Single-camera single-axis vision method applied to measure vibrations

Thomas Durand-Texte[a,b], Manuel Melon[a,*], Elisabeth Simonetto[b], Stéphane Durand[b], Marie-Héléne Moulet[c]

[a] *LAUM UMR CNRS 6613, avenue Olivier Messiaen, F-72085 Le Mans cedex 9, France*
[b] *Laboratoire Géomatique et Foncier, CNAM, 1 Bd Pythagore, 72000 Le Mans, France*
[c] *Centre de Transfert de Technologie du Mans, 20 rue Thalès de Milet, 72000 Le Mans, France*

**Abstract**

Increased interest has been witnessed for full-field techniques measuring vibrations. 3D vision methods coupled to two high-speed cameras have proven to be a valid solution to measure 3D displacements, notably with the Stereo Digital Image Correlation (SDIC) tools. The now conventional pseudo-stereo system with a single high-speed camera and a four-mirror adapter, generating two virtual cameras, may also be used, even if it is rather complex to operate and remains limited to small objects. In a logic of simplification of the protocol, the authors present here a set-up requiring a single high-speed camera and no mirrors, with the associated full-field single-axis vision method. The latter is logically designed to measure the vibrations of items whose displacements are locally along a single axis (usually normal to the surface). This paper reports firstly the results of the full-field measurement of the vibrations of a plate, validated by a comparison with those obtained with the four-mirror adapter set-up, and secondly the application to the full-field measurement of the vibrations of a tambourine. Thirdly, the conventional pseudo-stereo technique and the proposed vision method are compared and assessed, in order to establish their respective limits and potential complementarity. Finally, once the application of the method to plane objects is validated, measurements have been carried out on a non-planar object: a bent plate; the results obtained also validate the proposed approach for non-flat surfaces.

*Keywords:* vibration measurement, vision method, single high-speed camera

## Introduction

In order to measure vibrations, various approaches have been tried and tested over the past decades, ranging from single-point measurement devices (such as accelerometers [1] or usual laser vibrometers [2]) to indirect techniques, notably acoustic holography in the frequency domain [3, 4] or in the time domain [5, 6], time-domain near-field equivalence source imaging [7], time reversal imaging [8], deflectometry [9], the Force Analysis Technique [10]... Some drawbacks must generally be taken into account: intrusiveness, noise-sensitivity or complexity of implementation. More recently, direct optical full-field methods have been applied to measure vibrations: digital holography [11] or dynamic photogrammetry [12] for example. The latter has undeniable assets: it is non-intrusive, full-field, with a low sensitivity to acoustic noise, and it is easy to implement, even if the current related software is only partially adapted. In a context of shape or vibration measurement, 3D vision methods, as part of dynamic photogrammetry, are at the core of the approach presented in this paper.

High-speed cameras coupled to various methods, such as 3D vision or photogrammetry [12, 13, 14, 15, 16, 17, 18, 19, 20] or even videography [21, 22], have indeed been applied to measure structural vibrations, and sound [23]. One of the most widely used techniques for full-field 3D displacement measurement is the

*Corresponding author: manuel.melon@univ-lemans.fr

stereo-vision method, which requires two points of view that can be obtained from two cameras to perform vibration measurement with triangulation [24, 25] (see Fig. 1.a for a set-up sketch and Fig. 1.b for the triangulation principle).

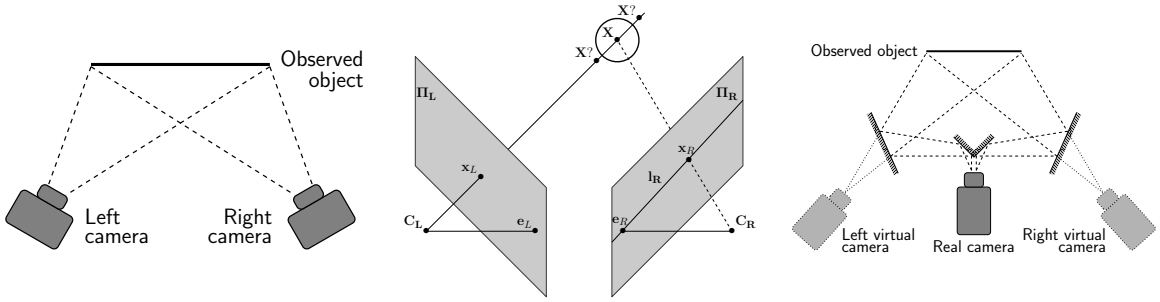


(a) (b) (c)

Figure 1: Principle of the measurement; (a) Sketch of the set-up with two cameras; (b) Triangulation; (c) Sketch of the set-up with a four-mirror adapter; with $\Pi_L$ and $\Pi_R$ the image planes of the left and right cameras, $C_L$ and $C_R$ the left and right camera centres, $x_L$ and $x_R$ the left and right images of the 3D point X, $l_R$ the epipolar line in the image plane of the right camera, $e_L$ and $e_R$ the images of the centres of the coordinate systems of the respectively right or left camera in the left or right image plane.

As high-speed cameras are expensive and difficult to synchronise neatly, alternatives have been studied and a valid solution has been borrowed from robotics: the now conventional single-camera pseudo-stereo system (see Fig. 1.c), for which the camera sensor is split into two halves, thanks to a four-mirror adapter [26, 27, 28], thus generating two virtual cameras. The interest of Digital Image Correlation (DIC) coupled to this pseudo-stereo set-up and a single high-speed camera in order to measure vibrations has recently been studied [29, 30, 31, 32]. The authors have previously tested the system and validated the protocol used to measure the vibrations of a plate by comparing the results to a reference technique (for more details see [33]).

Despite these promising results, it may be argued that the set-up is not particu1arly user-friendly (especially when positioning the central mirrors), that it takes up space and that the mirrors are particularly sensitive to vibrations and is thus difficult to use *in situ*. Moreover, with two views on a single camera, fewer pixels are available for each view (here half the resolution with image aliasing if the diaphragm of the objective is opened too widely [26]), which reduces measurement precision. The non-planarity of the mirrors may also lead to potential distortions for the initial shape measurement even though this does not seem to impact vibration measurement [33]. The main advantage remains, clearly, the use of a single high-speed camera for a stereo vision system applied to measure vibrations. In an attempt to simplify the set-up, the authors have already proposed a pseudo-stereo system with a two-mirror adapter only, which is more user-friendly and as precise in the case studied (for more details see [34]). Even if both pseudo-stereo set-ups allow measuring 3D displacements with a single camera, it should be borne in mind that vibrations often occur along a single axis: the local normal of the shape. A 3D measurement technique is thus not systematically required: a simplified technique, focused on the measurement of 1D displacement in 3D space, has thus been elaborated and is typically suited to vibro-acoustics. Indeed, in this field, the vibrations that are normal to the surface are of particular interest in order to calculate the acoustic radiation, with integral formalism for example, which only requires the knowledge of the normal velocity. As a reminder, the displacement of plates, shells and membranes, for instance, mainly or only occurs along the local normal of the surface: these items are consequently particularly well-suited objects of study in this context. To sum up, the aim of this paper is to propose a more user-friendly full-field vibration measurement method that allows to obtain the out-of-plane velocity field with a single high-speed camera. The targeted applications are the identification of the noisiest parts of a machine or the calculation of the radiated sound field from the normal velocity field.

This paper presents the single-camera single-axis (1D) vision method (section 1) and its validation on a plate (section 2) by comparing the results to those obtained with the conventional pseudo-stereo system with a four mirror adapter, considered here as a reference technique. The approach is then applied to measure the full-field vibrations of a tambourine and validated by comparing the results to those obtained with a laser vibrometer (section 3). In section 4 A comparison between the conventional pseudo-stereo system and the proposed method is carried out, in order to assess their respective limits and potential complementarity. Finally experimental tests on a bent plate are reported and establish the relevance of the proposed method applied this time to non-flat surfaces (section 5).

## 1. Presentation of the single-camera single-axis vision method

The technique presented here allows measuring single-axis displacements in 3D space, with a single high-speed camera and no mirrors. Indeed, if the initial 3D position of a point is known, and if the displacement is assumed to be along a single axis, a virtual mathematical line is sufficient to perform triangulation. The initial 3D location and orientation of the surface of the object are measured with snapshots captured by a high-speed camera and a simple (here mass-market) still camera. Then, the video of the vibrations is captured only with the high-speed camera (see Fig. 2). In this article, the high-speed camera is set at 12 500 fps and the focal length of its objective at 50 mm.

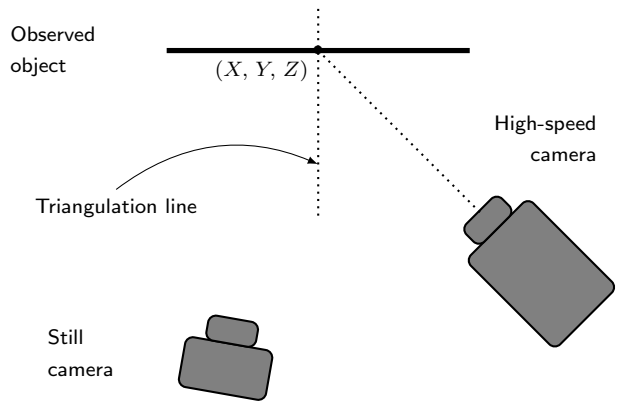


Figure 2: Sketch of the principle of the set-up without mirrors.

As a general rule, a 3D point of coordinates $(X, Y, Z)^T$ is firstly mapped to the pixel matrix of a camera with the following equation:

$$(k_i u_i, k_i v_i, k_i)^T = \mathbf{K_i R_i}((X, Y, Z)^T + \mathbf{T_i}), \tag{1}$$

with $\mathbf{K_i}$ the intrinsic camera matrix, $\mathbf{R_i}$ and $\mathbf{T_i}$ the rotation matrix and translation vector used to switch from the world coordinate system to the camera coordinate system, and $(u_i, v_i)$ the 2D coordinates in the pixel matrix. Note that $k_i$ is the distance from the point $(X, Y, Z)^T$ to the center of the camera $i$. Here, $\mathbf{K_1}$ $\mathbf{R_1}$, $\mathbf{T_1}$ and $(u_1, v_1)$ are linked to the first camera, and $\mathbf{K_2}$ $\mathbf{R_2}$, $\mathbf{T_2}$ and $(u_2, v_2)$ to the second one.

In order to perform triangulation, the point $(u_1, v_1)$ in the pixel matrix of the first camera is projected to the world 3D coordinate system and then onto the pixel matrix of the second camera:

$$(k_2 u_{1\to 2}, k_2 v_{1\to 2}, k_2)^T = \mathbf{K_2 R_2}(\mathbf{R_1}^{-1}\mathbf{K_1}^{-1}(k_1 u_1, k_1 v_1, k_1)^T - \mathbf{T_1} + \mathbf{T_2}). \tag{2}$$

The 3D location is obtained for the value of $k_1$ that minimises the distance between the 2D location $(u_2, v_2)$, paired to $(u_1, v_1)$, and the 2D location $(u_{1\to 2}, v_{1\to 2})$.

As vibrations mainly occur in a single direction in many cases, if the initial 3D position $(X, Y, Z)^T$ is known, a virtual triangulation line is defined by replacing data from the first camera in Eq. (2) by a vector and the 3D point $(X, Y, Z)^T$ (see Eq. (3)). This thus corresponds to a line (see Fig. 2):

$$(k_2 u_{1\to 2}, k_2 v_{1\to 2}, k_2)^T = \mathbf{K_2 R_2}(\mathbf{v_n}\delta_n + (X, Y, Z)^T + \mathbf{T_2}), \tag{3}$$

with $\mathbf{v_n}$ the unit vector in the world coordinate system of the triangulation line normal to the surface of the object and $\delta_n$ the value of the displacement. In the context of this paper, $\mathbf{K_2}$, $\mathbf{R_2}$ and $\mathbf{T_2}$ correspond to the parameters of the high-speed camera.

## 2. Validation of the method on a plate

A full-field measurement has been carried out on a plate and the results have been compared to those obtained with the conventional four-mirror adapter pseudo-stereo system, considered as reference in this section. Indeed, the four-mirror adapter pseudo-stereo system has been validated for vibration measurement in previous works [33, 35] by comparison of the results with those obtained with a laser vibrometer.

### *2.1. Protocol*

Pictures of the experimental zero-mirror set-up are shown in Fig. 3. The object of study is a 420 mm × 420 mm × 1.5 mm aluminium plate, suspended on an aluminium frame (see Fig. 3.a). The central measurement area is 180 mm × 180 mm large. A force is applied with a shaker, located at the back of the plate (see Fig. 3.b). The excitation signal is a swept sine, from 5 Hz to 1300 Hz in 2.25 seconds. Moreover, a mechanical impedance head (force sensor and accelerometer) is positioned between the plate and the shaker, in order to calculate the frequency response functions and to have a reference for each measurement point. An industrial camera (corresponding to the still camera in Fig. 2) is used to generate a stereo system, with the high-speed camera, in order to measure the initial shape. The high-speed camera is placed on one side of the plate, with an angle around 41°, and used to perform vibration measurement. Approximately 5,400 measurement points are used and the subsets, for both set-ups, correspond on the measured surface to discs measuring 6.6 mm in diameter.

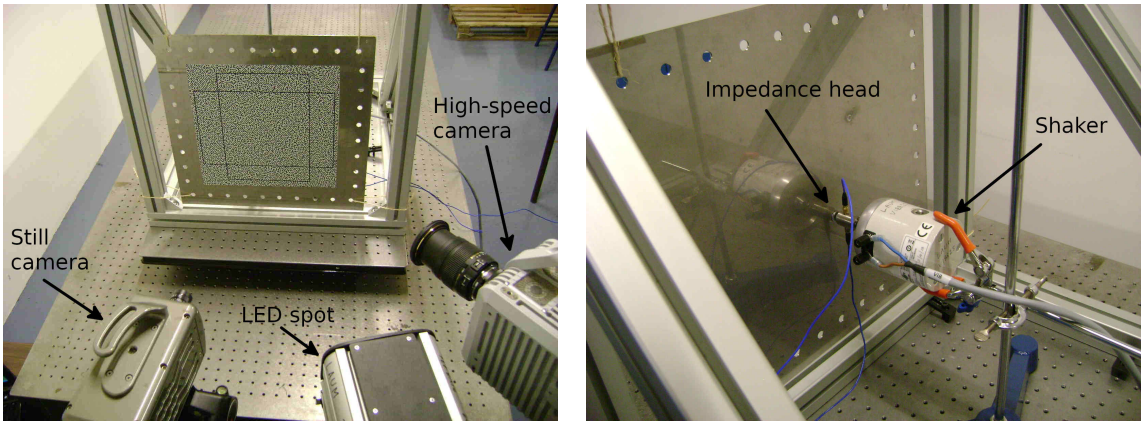


(a) (b)

Figure 3: (a) Picture of the experimental zero-mirror set-up with a suspended plate as object of study; (b) Picture of the shaker and the impedance head (color online).

### 2.2. Results

In order to have comparable data, the results of the vibration measurement of the plate, carried out with the proposed vision method for the axis normal to the surface, are displayed along with those obtained with the conventional set-up for the $z$ axis only. Note that both measurements have not been performed simultaneously, which however does not impact the results as the deformations observed are reproducible. Fig. 4 shows four examples of operational modal shapes (OMS) for both set-ups, chosen at 317 Hz, 594 Hz, 888 Hz and 1147 Hz to cover the full frequency band of interest. The correlation coefficients range from 99.2% to 99.9%: the OMSs obtained with these two methods are therefore in very good agreement.

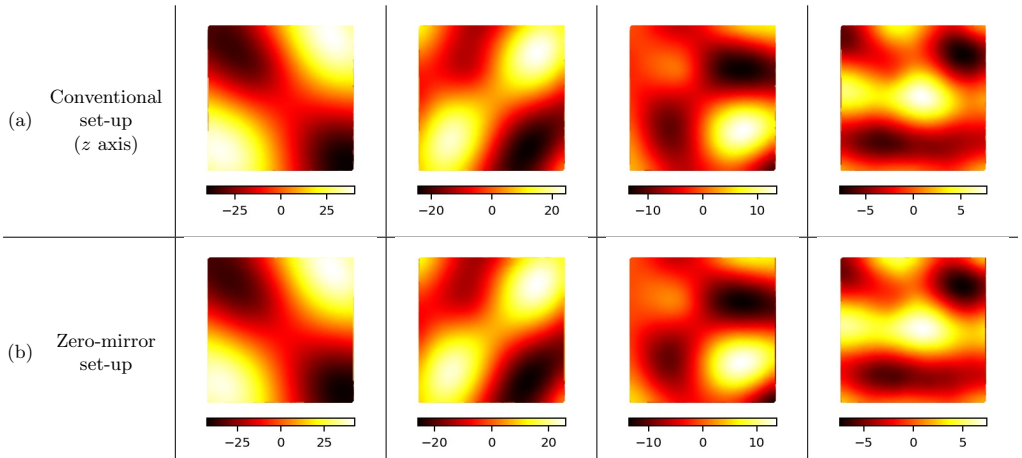


| | | | | |
|---|---|---|---|---|
| Freq. | 317 Hz | 594 Hz | 888 Hz | 1147 Hz |
| Corr. coef. | 99.9% | 99.9% | 99.4% | 99.2% |

Figure 4: OMSs in µm/N, (a) obtained with the conventional set-up and (b) calculated with the single-axis method at 317 Hz, 594 Hz, 888 Hz and 1147 Hz (color online).

## 3. Test on a tambourine

The technique is easy-to-use and well-suited to single-axis vibration measurement. Its interest lies in the possibility to measure non-reproducible vibrations. It has thus been tested on an object exclusively with a locally single-axis (non-reproducible) displacement: a tambourine. Note that the validation was obtained with only a single-point measurement with a laser vibrometer, as a full-field vibration measurement protocol including simultaneously the four-mirror adapter set-up and the proposed vision method could not be designed for lack of a second high-speed camera at disposal.

### 3.1. Protocol

A picture of the experimental set-up is shown in Fig. 5. The object is a 300 mm-large tambourine with a speckle pattern drawn on its membrane with a felt pen. A mass-market camera (corresponding to the still camera in Fig. 2) is used to generate a stereo system, with the high-speed camera, in order to measure the initial shape. The high-speed camera is placed on one side of the tambourine, with an angle around 42°. In addition, a laser vibrometer is placed in front of the membrane and is used as reference for a single point measurement. The impact is performed thanks to an electro-magnet mounted on a spring and the 3,000 measurement points allow tracking the temporal evolution of the impact on the membrane. The corresponding subsets are 6 mm-large discs on the measured surface. On Fig. 6, one can see, on the different snapshots, the impact propagating to the tambourine edge and then being reflected to gradually form a more complex pattern.

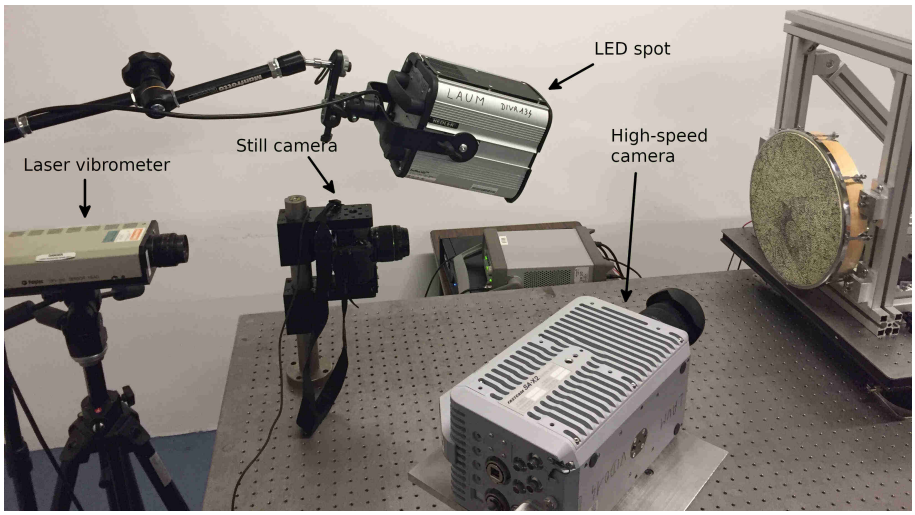


Figure 5: Picture of the experimental set-up (color online).

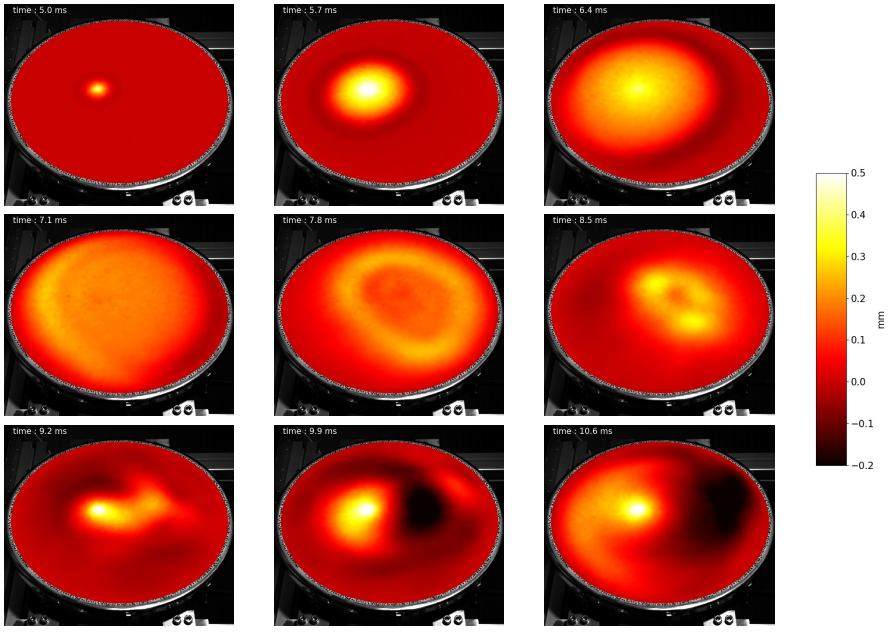


Figure 6: Temporal evolution of the impact (displacement); with a time step equal to 0.7 ms (color online).

### *3.2. Results*

From the data obtained at each point, operational deflection shapes (ODS) can be retrieved thanks to signal processing (see Fig. 7). Note that OMSs generally use a reference signal and are obtained with a frequency response function, with units in µm/N for the example of the plate, unlike ODSs for which only deformation is available. The units are thus in mm or µm in this case.

Finally, the displacement of a single point was measured simultaneously with the single-axis technique and a laser vibrometer. The location of the laser spot is shown in Fig. 8. The results show very good visual agreement in the frequency domain (see Fig. 9.a), with a correlation coefficient of 99,0% between the two curves, which validates the method once again. Note that, in the picture, noise is visible on the spectrum obtained with the vision method for the point corresponding to the location of the laser spot.

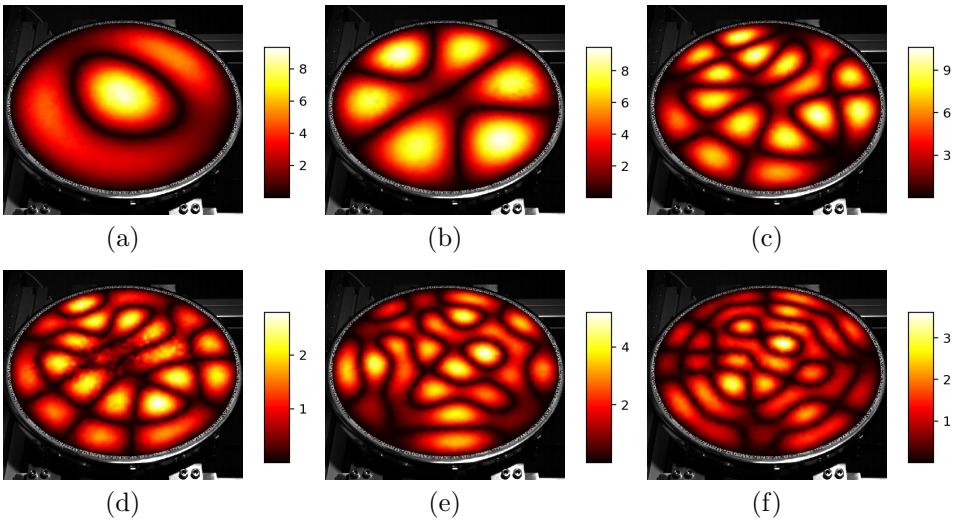


Figure 7: ODSs of the tambourine at different frequencies at (a) 361 Hz, (b) 412 Hz, (c) 768 Hz, (d) 858 Hz, (e) 950 Hz and (f) 1122 Hz, units are in $\mu$m (color online).

If this spectrum is compared to that obtained for an adjacent point (see Fig. 9.b), less noise is visible, which indicates that the saturation of the image induced by the laser spot generates noise at that particular location.


Figure 8: Image of the membrane with the drawn pattern and the position of the laser spot.

## 4. Comparison of both methods

The aim is now to establish the respective features and assess the main advantages and limits of the vision methods associated respectively to the conventional set-up and the zero-mirror set-up presented in this paper. In order to do so, simulations have first been carried out, with Blender software [36], to analyse, notably, the relative precision obtained while measuring the vibrations of a given object of study.

### *4.1. Blender simulations*

Simulation is a common way to obtain information about measurement precision or relative precision [37, 38, 39]. Here, images simulated with Blender software are thus used to compare both set-ups. A plate

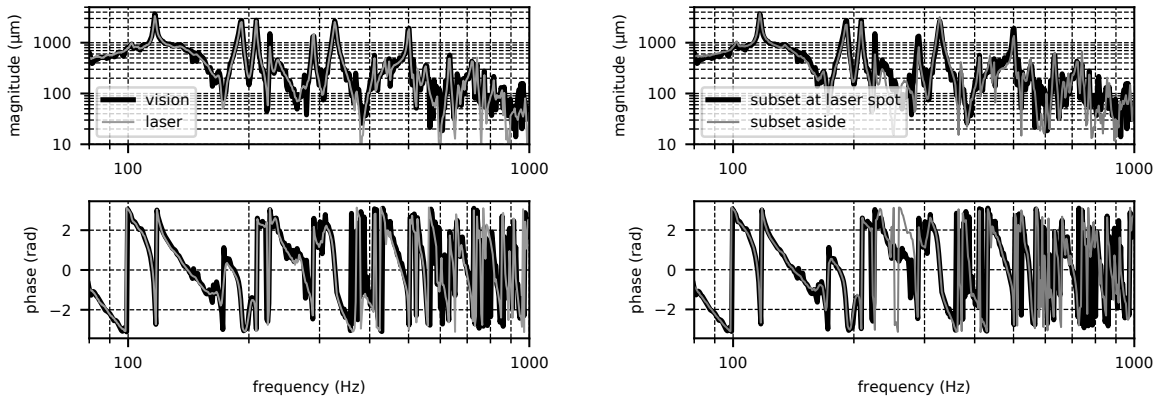


(a) (b)

Figure 9: (a) Spectra obtained with the vision method (*black*) and the laser vibrometer (*gray*); (b) Spectra obtained with the vision method at the laser spot (*black*) and aside (*gray*).

200 mm × 200 mm large is simulated with a single frequency vibration, decreasing with time, along the normal at each point. A photon noise [40] is added to all the images, to be as close as possible to real images, with 16,000 electrons for a fully loaded pixel sensor. The size of the speckle pattern has been adapted for the simulations of both set-ups so that the pattern of the subset tracked in all the images and used for the comparison may display similar features and notably similar patches (see Fig. 10). For the conventional four-mirror set-up, the subset corresponds to a 6 mm-large disc on the plate. For the set-up with no mirrors, the size of the pattern has been reduced by a factor 1.5 and the subset is a 4.4 mm-large disc, to obtain comparable data as more pixels are available for the view. The measurement point is chosen at the centre of the plate. The temporal evolution of the amplitude of the vibration is calculated and the results are compared for both set-ups: the dashed black, solid dark grey and solid light grey curves respectively correspond to the simulated amplitude, the amplitude calculated for the conventional set-up and the amplitude for the no-mirror set-up (see Fig. 11).

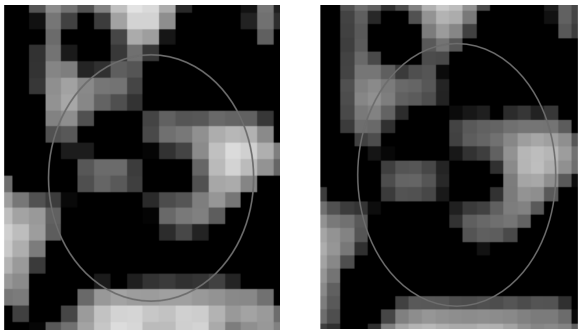

(a) (b)

Figure 10: Subsets tracked in the images; (a) Conventional set-up; (b) No-mirror set-up.

The four-mirror adapter and no-mirror set-ups present an error around 10% when the amplitude of vibration is around 5 $\mu$m and 2 $\mu$m respectively. The measurement curves shift away from the simulated curve when the amplitude of vibration is around 5 $\mu$m for the conventional set-up and around 0.5 $\mu$m for the proposed technique. Basically, the vibration-sensitive view of the no-mirror set-up has twice as many pixels available, compared to the virtual camera of the conventional pseudo-stereo system, as the whole pixel matrix is available, which certainly explains the higher precision of the method proposed in the case studied.

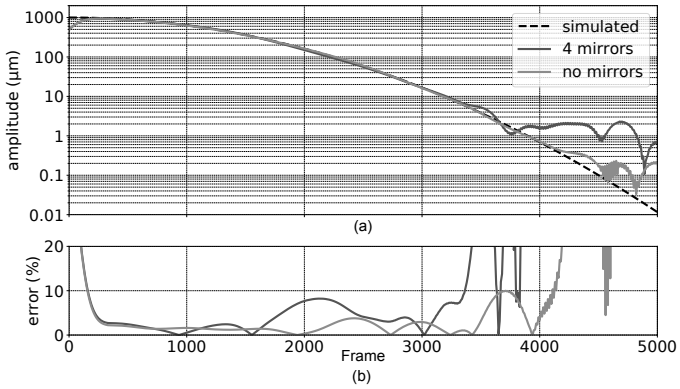


Figure 11: (a): simulated and calculated amplitudes for both set-ups. (b): errors for the two proposed set-ups.

Indeed, as pixel position in the image is non-linearly linked to 3D position, an increase in the number of pixels available per view strongly increases measurement precision. Note that these results are given as an indicative basis for comparison: one should bear in mind that the parameters of both set-ups are not exactly identical even if the approach minimizes the discrepancies as much as possible. Indeed, the percentage of use of the pixel matrix, the exact location of the measurement point and the ratio of the pattern size over the subset size are slightly different. Moreover, the data is obtained via simulations, and some imperfections may have not been taken into account, such as the non-flatness of the mirrors or the tangential optical distortion of the objective.

### *4.2. Discussion*

The results displayed in this section are obtained via simulation and experimentally. Firstly, Table 1 sums up the main features of both methods. The conventional set-up is clearly more complex to operate and logically designed preferably for vibration measurement carried out in a lab. Indeed, the mirrors are very light-weight, and thus very sensitive to vibrations as a small displacement of the mirrors virtually displaces the virtual camera and may thus add noise to the measurement. They require very stable, efficient anti-vibrating stands to minimise the impact of vibration. On the contrary, the no-mirror set-up can be used almost anywhere, as no stand is required (just a tripod for the camera). The sensitivity of the set-up to vibration is much lower and often negligible with a steady tripod. The main difference between the two methods is basically the nature of the measured displacement: the four-mirror adapter set-up provides 3D measurement, unlike the no-mirror one, which is typically suited to 1D measurement. In terms of accuracy, the proposed method, with no mirrors, in the case studied, is more precise, with smaller measurement points on the object of study as the whole matrix of pixels is available. Secondly, Table 2 presents the values of the correlation coefficients calculated for the operational modal shapes of a vibrating plate (see section 2) obtained with the zero-mirror set-up, compared with those from the four-mirror set-up ($z$ axis), considered here as a reference. The values are globally above 98%, indicating that the two methods give very similar results.

## 5. Application to a curved plate

In the previous sections, the proposed method has been validated thanks to:

- measurements of the vibrations of a plane plate and a comparison of the results with those obtained with the conventional pseudo-stereo set-up;

Table 1: General comparison of both set-ups

| Method | conventional set-up | zero-mirror set-up |
|---|---|---|
| Nature of the measurable displacement | multi-axis | single-axis |
| Maximum measurement surface | $\approx$ 300 mm $\times$ 300 mm | very large |
| Number of pixels per view | half resolution | full resolution |
| Limit amplitude* for a 10% error (relative to the measured surface width) | $\approx$ 1/40,000 | $\approx$ 1/100,000 |
| Detection limit* (relative to the measured surface width) | $\approx$ 1/40,000 | $\approx$ 1/400,000 |
| User-friendliness | $--$ | $+$ |
| Space required for the set-up | large | small |

* for a 1,024 $\times$ 1,024 pixel camera

Table 2: Correlation coefficients (in %) for the OMSs obtained with the proposed method, compared with those obtained with the conventional set-up ($z$ axis)

| Frequency (Hz) | 222 | 317 | 339 | 490 | 594 | 888 | 934 | 1036 | 1147 | 1245 |
|---|---|---|---|---|---|---|---|---|---|---|
| Correlation coefficient (%) | 99.7 | 99.9 | 99.9 | 99.6 | 99.9 | 99.4 | 98.1 | 99.8 | 99.2 | 99.2 |

- measurements of deformations induced by an impact on the membrane of a tambourine, and a comparison of the data with those of a single point laser vibrometer;
- imaging of a vibrating plate, simulated with Blender software, highlighting the benefits of the proposed method, compared to the conventional pseudo-stereo system.

As evidenced previously, the proposed method allows measuring locally single axis displacement, in a known 3D direction. In order to validate the approach, the systems studied so far were plane. This section now focuses on a final validation, obtained by measuring a non-planar surface, namely a bent plate, clamped on its four corners. Before being bent, the plate was 350 mm long, 250 mm wide and 1.5 mm thick. The dimensions of the measured area are $\approx$ 290 mm $\times$ 200 mm and correspond to a speckle pattern printed on a A4 sticker. Pictures of the experimental set-up are shown in Fig. 12. The cameras used are the same as for the tambourine experiment.

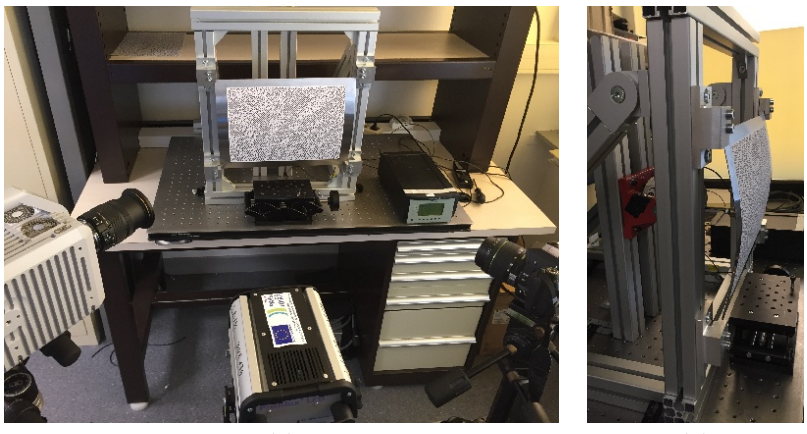

(a) (b)

Figure 12: Pictures of the experiment: (a) set-up; (b) side view of the plate (color online).

It may be worth reminding that the first step consists in measuring the shape of the measured surface in order to estimate firstly the position, relative to the high-speed camera, of each measurement point and

secondly the corresponding local normals corresponding to the unit vector $\mathbf{v_n}$ in Eq. (3). The measured shape, the epipolar distance map and the map showing the angle between the local normals and the normal to the average plane are displayed in Fig. 13(a), (b) et (c) respectively. The average epipolar distance is 0.034 pixels, with a standard deviation equal to 0.030 pixels. Note that higher values are observed in the corners on the right of the plate, which points out the limits of the calibration of the stereo system.

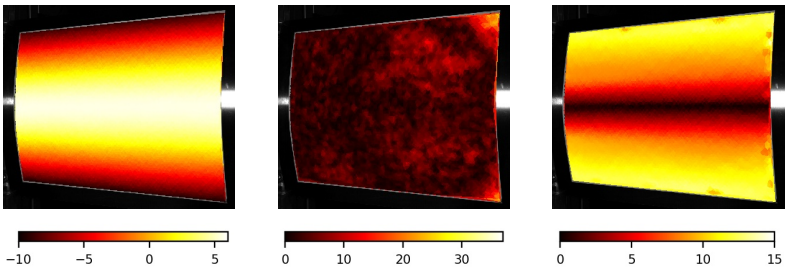


(a) (b) (c)

Figure 13: Results of the shape measurement: (a) depth (in mm); (b) epipolar distances (in pixels/100); (c) angles between the local normals and the normal to the average plane (in degrees); (color online).

As the phenomena measured here are repeatable, single frequency measurements are carried out for three modes detected thanks to the admittance curve measured with an impedance head (see Fig. 12): at 68 Hz, 228 Hz and 390 Hz. For each measurement, 500 images are captured. The first step so as to validate the proposed approach is to check if the displacements of the surface are indeed along the measured local normals. The estimated 2D positions of a measurement point, tracked in the video corresponding to the mode at 68 Hz, are plotted in Fig. 14 (a) along with the projection of the local normal onto the image coordinate system. A good agreement is visible, and the corresponding triangulated displacements, plotted with time wrapped according to the excitation period and shown in Fig. 14 (b), is sinusoidal.

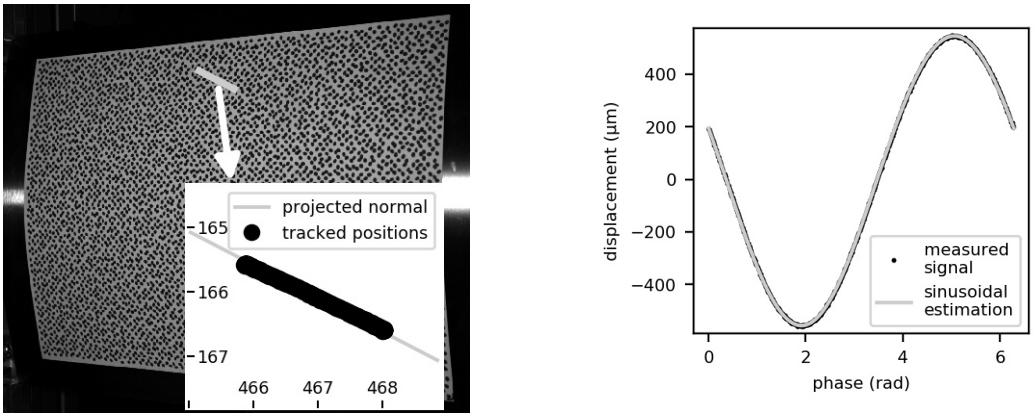


(a) (b)

Figure 14: (a) Image of the local normal projected onto the image plane of the high-speed camera and tracked 2D positions for a sinusoidal excitation at $f0 = 68$ Hz; (b) triangulated signal and sinusoidal estimation.

The vibration field, estimated over $\approx$ 4,000 measurement points, is displayed in Fig. 15 and exhibits a very good signal to noise ratio, even for vibration amplitudes of a few micrometers at 390 Hz. The amplitudes of the input force, at 68 Hz, 228 Hz and 390 Hz, are 0.36 N, 0.46 N and 0.16 N respectively.

Finally, the presented experiment, once again, validates the approach, this time for a non-flat object. Indeed, the displacements induced by vibrations actually occur along the local normal and the proposed

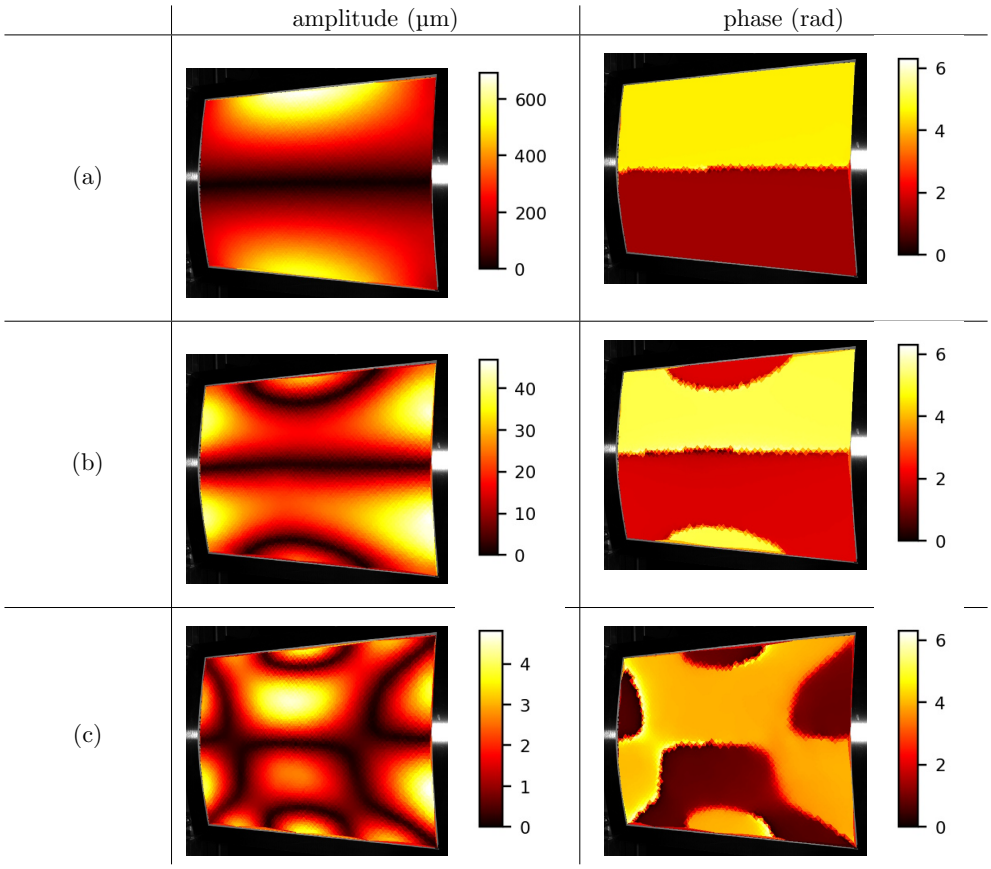


Figure 15: Estimated vibrational displacement field for a single frequency excitation at (a) 68 Hz, (b) 228 Hz and (c) 390 Hz (color online).

triangulation process corrects the distortions due to the perspective projection. The measured kinematic fields visually present a very good signal to noise ratio, even for a few micrometers of amplitude.

## 6. Conclusion

This paper has presented a full-field vision method designed to measure the single-axis vibrations of planar and non-planar objects, displaying repeatable or non-repeatable displacements along the normal of the surface. Firstly, the approach has been tested on a suspended plate, whose vibratory behaviour is globally along a single axis after excitation. The correlation coefficients calculated for the OMSs obtained on the one hand with the proposed method and on the other hand with the conventional four-mirror adapter pseudo-stereo system (considered here as reference for the $z$ axis) are above 98% and thus validate the proposed vision method for full-field vibration measurement.

Secondly, the method has been tested on an object of study matching the established requirements: a tambourine, whose displacement is, indeed, exclusively locally along a single axis. The results have been compared to those obtained with a laser vibrometer and are in agreement for one measurement point. Subsequent full-field measurement allowed following the evolution of an impact on the membrane, *i.e.* of a non-repeatable transitory phenomenon, up to 2 kHz and down to a few micrometers of amplitude. Note that the membrane of a tambourine is basically an extremely light-weight structure. The results achieved with the single-camera single-axis vision method presented in this paper could not have been obtained with most of the other techniques available, as the objective is to measure full-field non-repeatable non-stationary

phenomena. Indeed, the accelerometers used for reverse techniques for instance, would extensively modify the vibratory behaviour of the membrane and scanning laser Doppler vibrometers are not compatible with non-repeatable phenomena, for instance. Similarly, the membrane is not reflective enough to carry out measurement with approaches such as deflectometry or digital holography, not to mention the measurement area which may be challenging for vibration measurement with the latter technique.

Thirdly, the measurements carried out on a curved plate highlight the possibility to use the proposed approach for non-planar surfaces. Indeed, the experiment stage gave evidence that the displacements induced by vibrations actually occur along the local normal and that the proposed method allows measuring vibrations of a few micrometers of amplitude with a satisfactory signal to noise ratio. Yet, the method relies on the assumption that displacement occurs along the local normal: this must be verified for each system, as it was done for the curved plate. Moreover, with a single viewpoint/camera, the measurement sensitivity is linked to the angle between the displacement axis and the line perpendicular to the image plane. The choice of an object like a cone for example with significant angles in several directions can end up in reduced sensitivity areas for/because the measured surface can be locally almost parallel to the image plane.

Finally, it must be borne in mind that vision methods require a pattern to perform shape and deformation measurements. The pattern can be obtained with paint or glued stickers, which potentially impacts the dynamic behaviour of the tested object, even if this impact is usually considered as negligible and neglected. In this paper, for simplicity, the patterns applied have been made with glued stickers for the aluminium plates, which are at least 1.5 mm thick; other solutions could have been chosen, like spraying paint or using a stencil for example. For the membrane of the tambourine, the ink that was manually applied is lighter than paint, all the more so since a very thin layer was applied: this option thus seemed the most relevant. One could argue that scanning laser Doppler vibrometers (SLDV) do not require any pattern on the measured surface. This is indeed the case. Yet, the devices are even more expensive than two very high-speed cameras. Moreover, measurements with SLDV usually last several hours, compared to only a few seconds for vision methods, with potentially induced heating. They are also limited to reproducible phenomena for kinematic field measurement of surfaces. In the end, vision methods and other methods like SLDV may be considered as complementary, with specific advantages and drawbacks on both sides, depending on the nature of the measured surfaces and the studied phenomena.

In brief, the vision method presented in this paper is a full-field non-contact technique designed to measure the locally 1D displacement of an object. It offers a higher number of pixels for the vibration-sensitive view (compared to other pseudo-stereo systems), which allows retrieving OMSs or ODSs with amplitudes of displacement around a 1/100,000th and a detection limit around a 1/400,000th of the size of the measurement surface. The set-up is in essence simpler and more user-friendly than the conventional pseudo-stereo system for example, as no mirror is required: the second view needed to triangulate the data is replaced by a mathematical line. The technique is accessible and also less expensive. Yet, unlike the conventional system which provides 3D measurement, the proposed vision method is designed for an exclusively locally 1D displacement. The approach, validated on a plate, a tambourine and a bent plate, seems to give more accurate results than the conventional single camera set-up, for the cases studied. Both vision methods are finally complementary alternatives for vibration measurement, depending on the objective: either single-axis or multi-axis displacement, either small or larger objects, either in a laboratory or *in situ*.

**Acknowledgements**

The work presented here is supported by the institute “Le Mans Acoustique” and funded by the “Pays de la Loire” region and the “European Regional Development Fund”.

## References


[1] B. Anders, Noise and Vibration Analysis: Signal Analysis and Experimental Procedures, Wiley, 2011 (2011).

[2] F. Frank, J. Walker, Advanced Applications in Acoustics, Noise and Vibration, CRC Press, 2004 (2004).

[3] J. D. Maynard, E. G. Williams, Y. Lee, Nearfield acoustic holography: I. theory of generalized holography and the development of nah, J. Acoust. Soc. Am. 78 (1985) 1395–1413 (1985). doi:10.1121/1.392911.

[4] E. G. Williams, Fourier Acoustics Sound radiation and Near field Acoustical Holography, San Diego, 1999 (1999).

[5] J. Hald, Time domain acoustical holography and its applications, Sound and vibration 35 (2) (2001) 16–25 (2001).

[6] J.-H. Thomas, V. Grulier, P. Paillasseur, J.-C. Pascal, J.-C. Le Roux, Real-time near-field acoustic holography for continuously visualizing nonstationary acoustic fields, J. Acoust. Soc. Am. 128 (2010) 3554–67 (2010). doi:10.1121/1.3504656.

[7] M. Bai, J.-H. Lin, Source identification system based on the time-domain nearfield equivalence source imaging: Fundamental theory and implementation, J. Sound Vib. 307 (1-2) (2007) 202–225 (2007). doi:10.1016/j.jsv.2007.06.025.

[8] S. Lobréau, E. Bavu, M. Melon, Hemispherical double-layer time reversal imaging in reverberant and noisy environments at audible frequencies, The Journal of the Acoustical Society of America 137-2 (2015) 785–796 (Fev 2015). doi:10.1121/1.4906164.

[9] A. Berry, O. Robin, Identification des excitations sur des panneaux par la mesure de leur réponse vibratoire et la méthode des champs virtuels, in: CFA 2016, Le Mans, France, 2016 (2016).

[10] C. Pézerat, J.-L. Guyader, Identification of vibration sources, Applied Acoustics 61 (2000) 309–324 (2000). doi:10.1016/S0003-682X(00)00036-0.

[11] J. Poittevin, P. Picart, C. Faure, F. Gautier, C. Pézerat, Multi-point vibrometer based on high-speed digital in-line holography, Appl. Opt. 54 (11) (2015) 3185–3196 (Apr 2015). doi:10.1364/AO.54.003185.

[12] J. Baqersad, P. Poozesh, C. Niezrecki, P. Avitabile, Photogrammetry and optical methods in structural dynamics - A review, Mechanical Systems and Signal Processing 86 (2017) 17–34 (Mar. 2017). doi:10.1016/j.ymssp.2016.02.011.

[13] T. Siebert, T. Becker, K. Spiltthof, I. Neumann, R. Krupka, High-speed digital image correlation: error estimations and applications, Optical Engineering 46-5 (2007) 051004 (2007). doi:10.1117/1.2741217.

[14] V. Tiwari, M. A. Sutton, S. R. McNeill, Assessment of high speed imaging systems for 2d and 3d deformation measurements: Methodology development and validation, Experimental Mechanics 47 (4) (2007) 561–579 (Aug 2007). doi:10.1007/s11340-006-9011-y.

[15] M. N. Helfrick, C. Niezrecki, P. Avitabile, T. Schmidt, 3d digital image correlation methods for full-field vibration measurement, Mechanical Systems and Signal Processing 25 (3) (2011) 917 – 927 (2011). doi:10.1016/j.ymssp.2010.08.013.

[16] C. Warren, C. Niezrecki, P. Avitabile, Optical non-contacting vibration measurement of rotating turbine blades ii, in: T. Proulx (Ed.), Structural Dynamics and Renewable Energy, Volume 1, Springer New York, New York, NY, 2011, pp. 39–44 (2011).

[17] T. Beberniss, T. Eason, S. Spottswood, High-speed 3d digital image correlation measurements of long-duration random vibration; recent advancements and noted limitations, in: Proceedings, International Conference on Noise and Vibration Engineering (ISMA), KatholiekeUniversiteit Leuven, Belgium, 2012 (2012).

[18] E. Zappa, P. Mazzoleni, A. Matinmanesh, Uncertainty assessment of digital image correlation method in dynamic applications, Optics and Lasers in Engineering 56 (2014) 140 – 151 (2014). doi:10.1016/j.optlaseng.2013.12.016.

[19] C. Cameron, J. Sirohi, D. Uehara, Transient hub loads and blade deformation of a mach-scale coaxial rotor in hover, in: 56th AIAA/ASCE/AHS/ASC Structures, Structural Dynamics, and Materials Conference, 2015 (01 2015).

[20] T. Lundstrom, J. Baqersad, C. Niezrecki, Monitoring the dynamics of a helicopter main rotor with high-speed stereophotogrammetry, Experimental Techniques 40 (3) (2016) 907–919 (Jun 2016). doi:10.1007/s40799-016-0092-y.

[21] C. V. Karsen, T. Bouman, G. Gwaltney, Operating Deflection Shapes of a Violin String via High Speed/High Resolution Videography, in: R. Allemang, J. D. Clerck, C. Niezrecki, A. Wicks (Eds.), Topics in Modal Analysis, Volume 7, Conference Proceedings of the Society for Experimental Mechanics Series, Springer New York, 2014, pp. 637–644 (2014). doi:10.1007/978-1-4614-6585-0_61.

[22] J. G. Chen, N. Wadhwa, Y.-J. Cha, F. Durand, W. T. Freeman, O. Buyukozturk, Modal identification of simple structures with high-speed video using motion magnification, Journal of Sound and Vibration 345 (2015) 58–71 (2015). doi:10.1016/j.jsv.2015.01.024.

[23] A. Davis, M. Rubinstein, N. Wadhwa, G. J. Mysore, F. Durand, W. T. Freeman, The visual microphone: Passive recovery of sound from video, ACM Trans. Graph. 33 (4) (2014) 79:1–79:10 (jul 2014). doi:10.1145/2601097.2601119.

[24] M. Sutton, J.-J. Orteu, H. W. Schreier, Image Correlation for Shape, Motion and Deformation Measurements. Basic Concepts, Theory and Applications, Springer US, 2009 (01 2009).

[25] R. I. Hartley, A. Zisserman, Multiple View Geometry in Computer Vision, 2nd Edition, Cambridge University Press, 2004 (2004).

[26] M. Inaba, T. Hara, H. Inoue, A stereo viewer based on a single camera with view-control mechanisms, in: Proceedings of 1993 IEEE/RSJ International Conference on Intelligent Robots and Systems, IROS 1993, Tokyo, Japan, July 26 - 30, 1993, 1993, pp. 1857–1865 (1993).

[27] R. Wang, X. Li, Y. Zhang, Analysis and optimization of the stereo-system with a four-mirror adapter, Journal of the European Optical Society - Rapid publications 3 (0) (2008). doi:10.2971/jeos.2008.08033.

[28] J. Li, X. Dan, W. Xu, Y. Wang, G. Yang, L. Yang, 3d digital image correlation using single color camera pseudo-stereo system, Optics & Laser Technology 95 (2017) 1 – 7 (2017). doi:10.1016/j.optlastec.2017.03.030.

[29] P. Castellini, P. Chiariotti, M. Martarelli, E. Zappa, A. Lavatelli, Experimental modal analysis on vibration data measured by digital image correlation, in: J. M. Harvie, J. Baqersad (Eds.), Shock & Vibration, Aircraft/Aerospace, Energy Harvesting, Acoustics & Optics, Volume 9, Springer International Publishing, Cham, 2017, pp. 285–291 (2017).

[30] T. G. White, J. R. W. Patten, K.-H. Wan, A. D. Pullen, D. J. Chapman, D. E. Eakins, A single camera three-dimensional digital image correlation system for the study of adiabatic shear bands, Strain 53 (3) (2017). doi:10.1111/str.12226.
[31] L. Yu, B. Pan, Single-camera high-speed stereo-digital image correlation for full-field vibration measurement, Mechanical Systems and Signal Processing 94 (2017) 374–383 (2017). doi:10.1016/j.ymssp.2017.03.008.
[32] L. Yu, B. Pan, Full-frame, high-speed 3d shape and deformation measurements using stereo-digital image correlation and a single color high-speed camera, Optics and Lasers in Engineering 95 (2017) 17 – 25 (2017). doi:10.1016/j.optlaseng.2017.03.009.
[33] T. Durand-Texte, E. Simonetto, S. Durand, M. Melon, M.-H. Moulet, Vibration measurement using a pseudo-stereo system, target tracking and vision methods, Mechanical Systems and Signal Processing 118 (2019) 30–40 (March 2019). doi:10.1016/j.ymssp.2018.08.049.
[34] T. Durand-Texte, M. Melon, E. Simonetto, S. Durand, M.-H. Moulet, 3d vision method applied to measure the vibrations of non-flat items with a two-mirror adapter, Journal of Physics: Conference Series 1149 (2018) 012008 (dec 2018). doi:10.1088/1742-6596/1149/1/012008.
[35] T. Durand-Texte, M. Melon, E. Simonetto, S. Durand, M.-H. Moulet, Vision methods applied to measure the displacement of loudspeaker membranes, in: Audio Engineering Society Convention 144, 2018 (May 2018).
[36] Blender Foundation, Blender a 3D modelling and rendering package.
URL http://www.blender.org
[37] B. Pan, H. Xie, Z. Wang, K. Qian, Z. Wang, Study on subset size selection in digital image correlation for speckle patterns, Optics express 16 (2008) 7037–48 (06 2008). doi:10.1364/OE.16.007037.
[38] R. Balcaen, P. Reu, P. Lava, D. Debruyne, Stereo-dic uncertainty quantification based on simulated images, Experimental Mechanics 57 (6) (2017) 939–951 (2017). doi:10.1007/s11340-017-0288-9.
[39] C. Sebastian, E. López-Alba, E. Patterson, A comparison methodology for measured and predicted displacement fields in modal analysis, Journal of Sound and Vibration 400 (2017) 354 – 368 (2017). doi:10.1016/j.jsv.2017.03.024.
[40] A. Foi, M. Trimeche, V. Katkovnik, K. Egiazarian, Practical poissonian-gaussian noise modeling and fitting for single-image raw-data, IEEE Transactions on Image Processing 17 (10) (2008) 1737–1754 (Oct 2008). doi:10.1109/TIP.2008.2001399.

**Figure(s)**

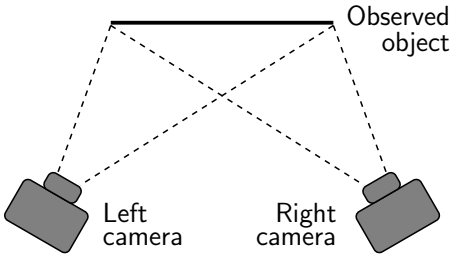
Observed
object
Left
camera
Right
camera

(a)

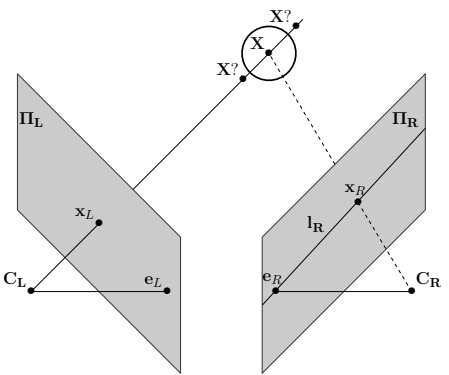
X?
X
X?
Π_L
Π_R
x_L
x_R
l_R
C_L
e_L
e_R
C_R

(b)

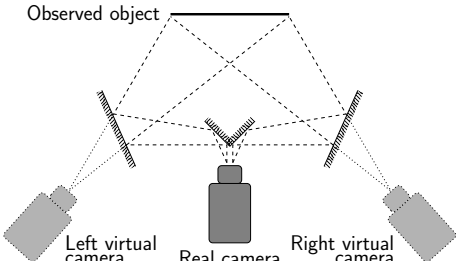
Observed object
Left virtual
camera
Real camera
Right virtual
camera

(c)

**Figure(s)**

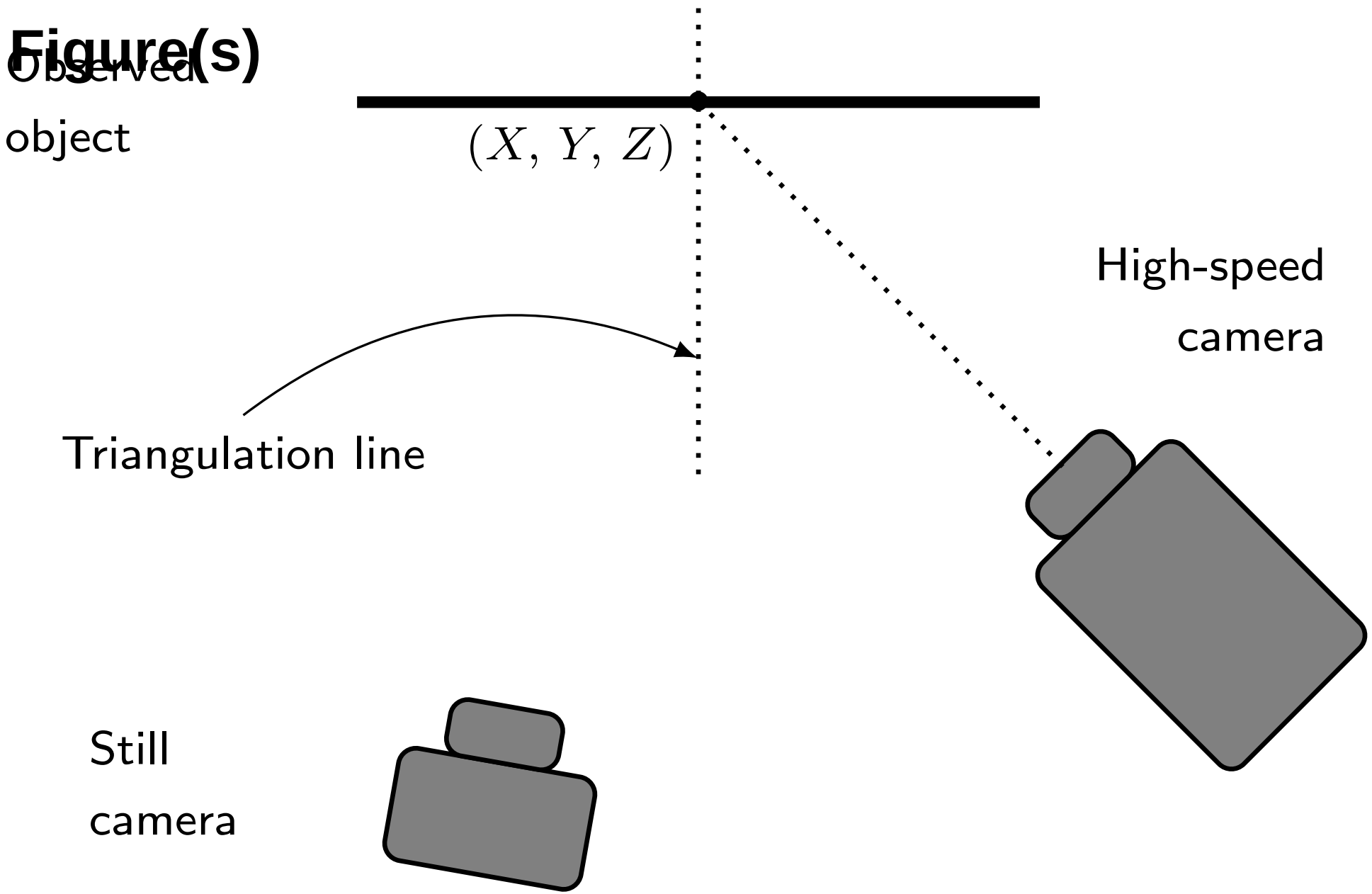
Observed
object
$(X, Y, Z)$
High-speed
camera
Triangulation line
Still
camera

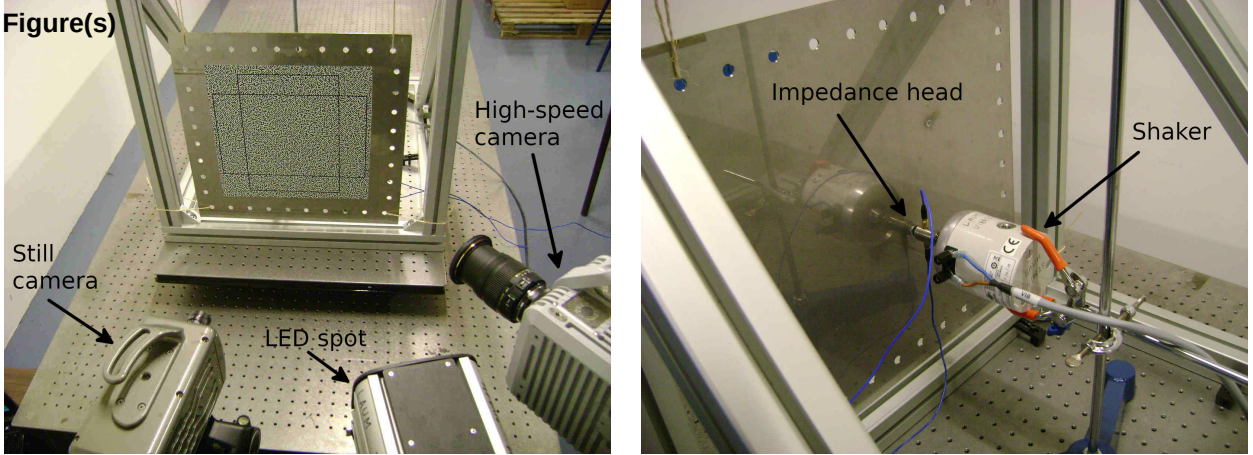
Figure(s)
High-speed camera
Still camera
LED spot
Impedance head
Shaker

(a) (b)

**Figure(s)**

| | | | | |
|---|---|---|---|---|
| (a) Conventional set-up ($z$ axis) | 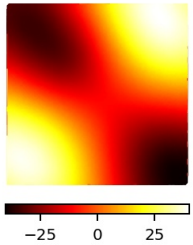  | 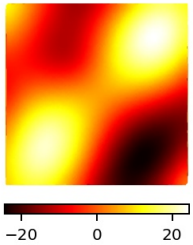  | 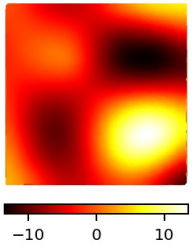  | 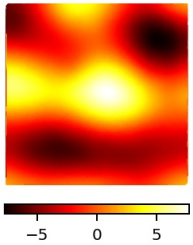  |
| (b) Zero-mirror set-up | 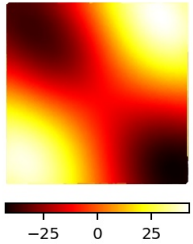  | 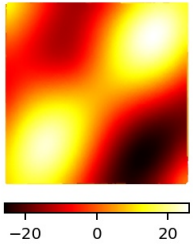  | 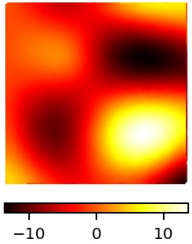  | 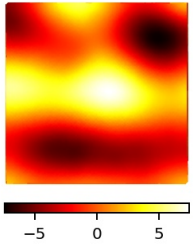  |
| Freq. | 317 Hz | 594 Hz | 888 Hz | 1147 Hz |
| Corr. coef. | 99.9% | 99.9% | 99.4% | 99.2% |

**Figure(s)**

**Click here to download high resolution image**

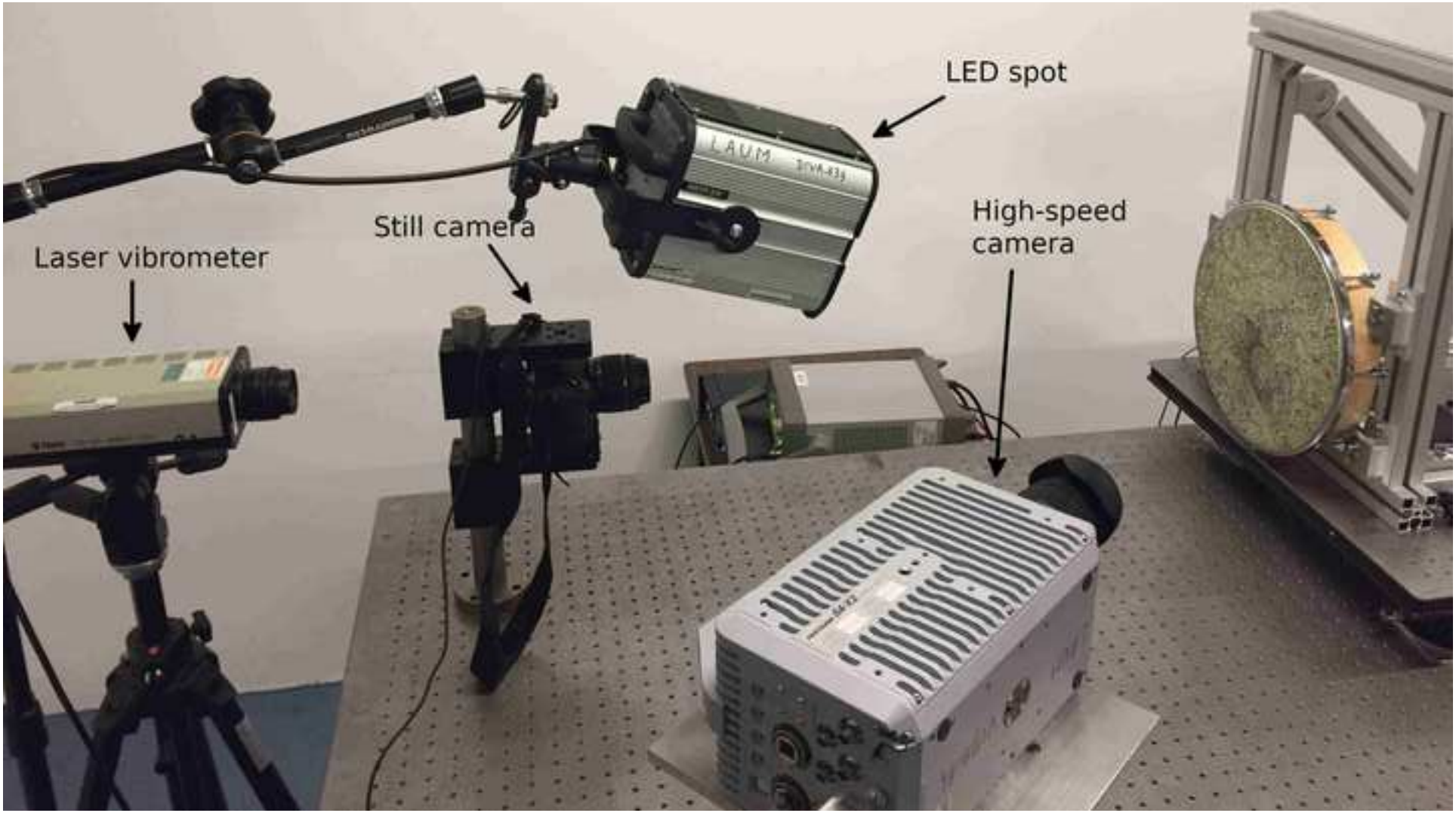

Figure(s)

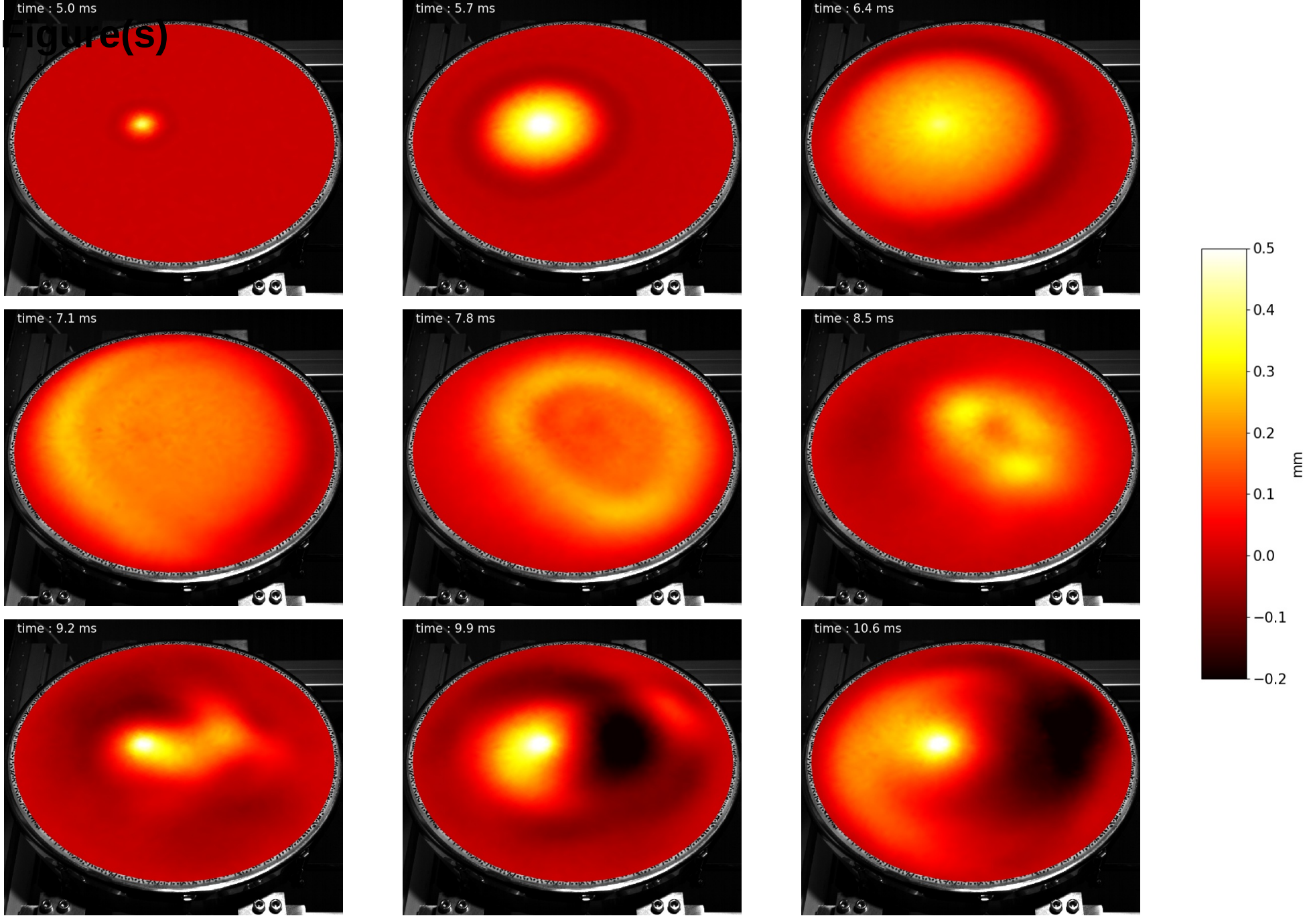
time : 5.0 ms
time : 5.7 ms
time : 6.4 ms
time : 7.1 ms
time : 7.8 ms
time : 8.5 ms
time : 9.2 ms
time : 9.9 ms
time : 10.6 ms
0.5
0.4
0.3
0.2
0.1
0.0
−0.1
−0.2
mm

Figure(s)

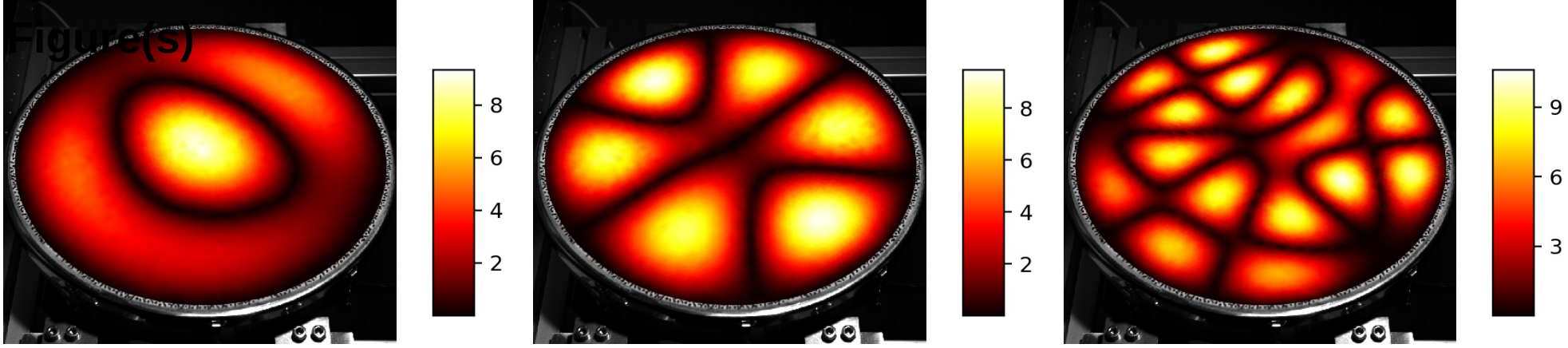


(a) (b) (c)

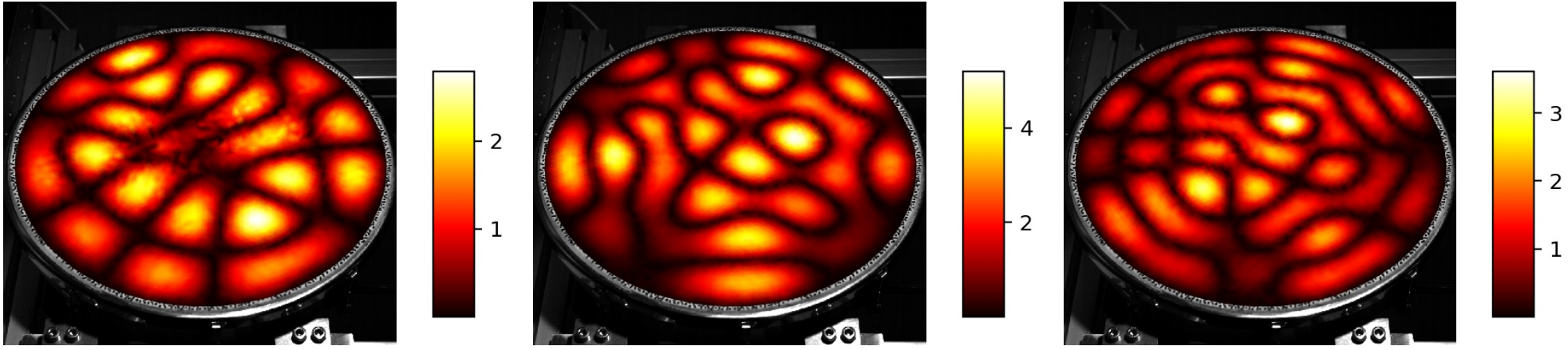


(d) (e) (f)

**Figure(s)**

**Click here to download high resolution image**

Figure(s)

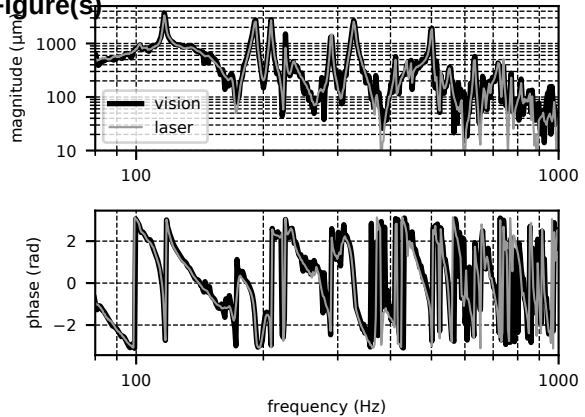
magnitude (µm)
1000
100
10
vision
laser
100
1000
phase (rad)
2
0
−2
100
1000
frequency (Hz)

(a)

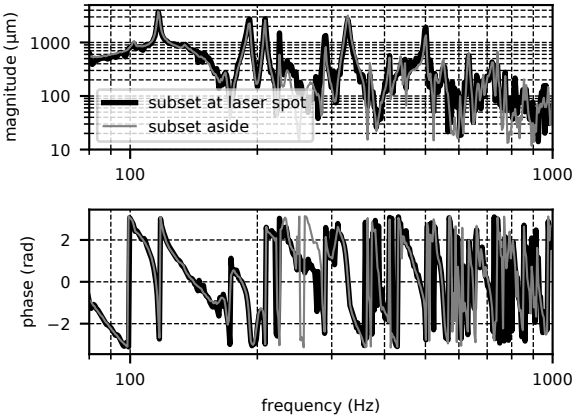
magnitude (µm)
1000
100
10
subset at laser spot
subset aside
100
1000
phase (rad)
2
0
−2
100
1000
frequency (Hz)

(b)

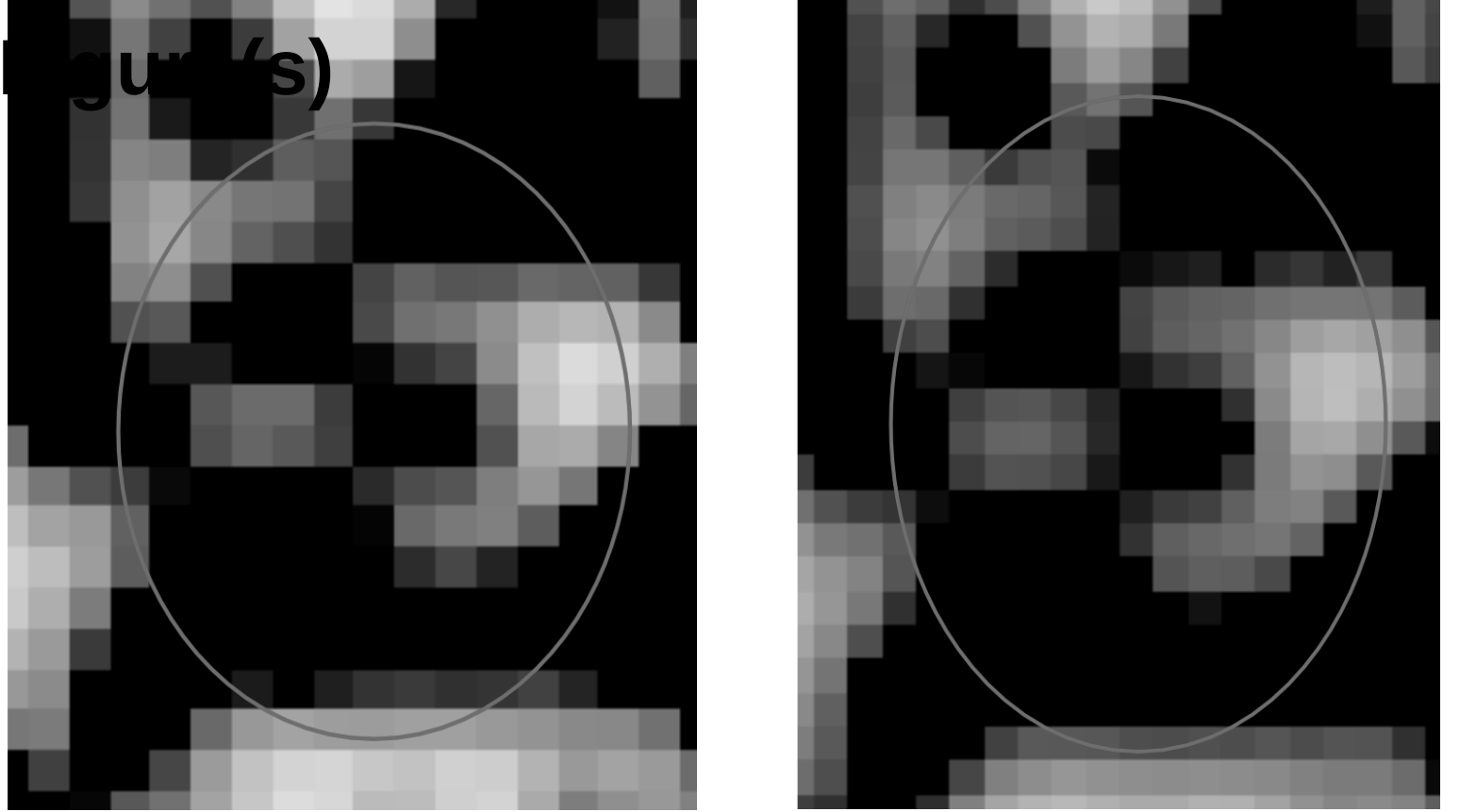

(a) (b)

Figure(s)

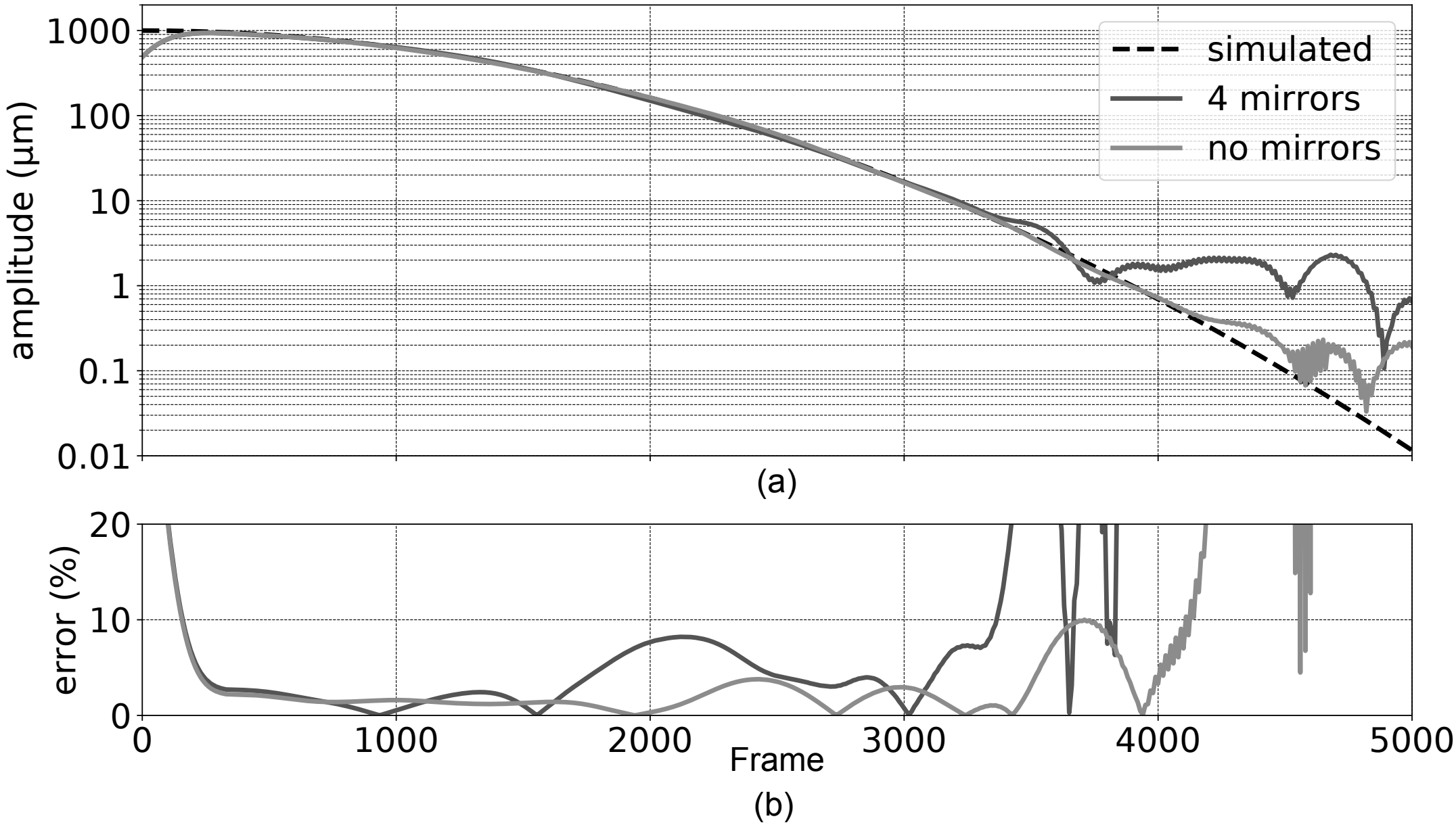
1000
100
10
1
0.1
0.01
amplitude (μm)
simulated
4 mirrors
no mirrors
(a)
20
10
0
error (%)
0
1000
2000
3000
4000
5000
Frame
(b)

Figure(s)

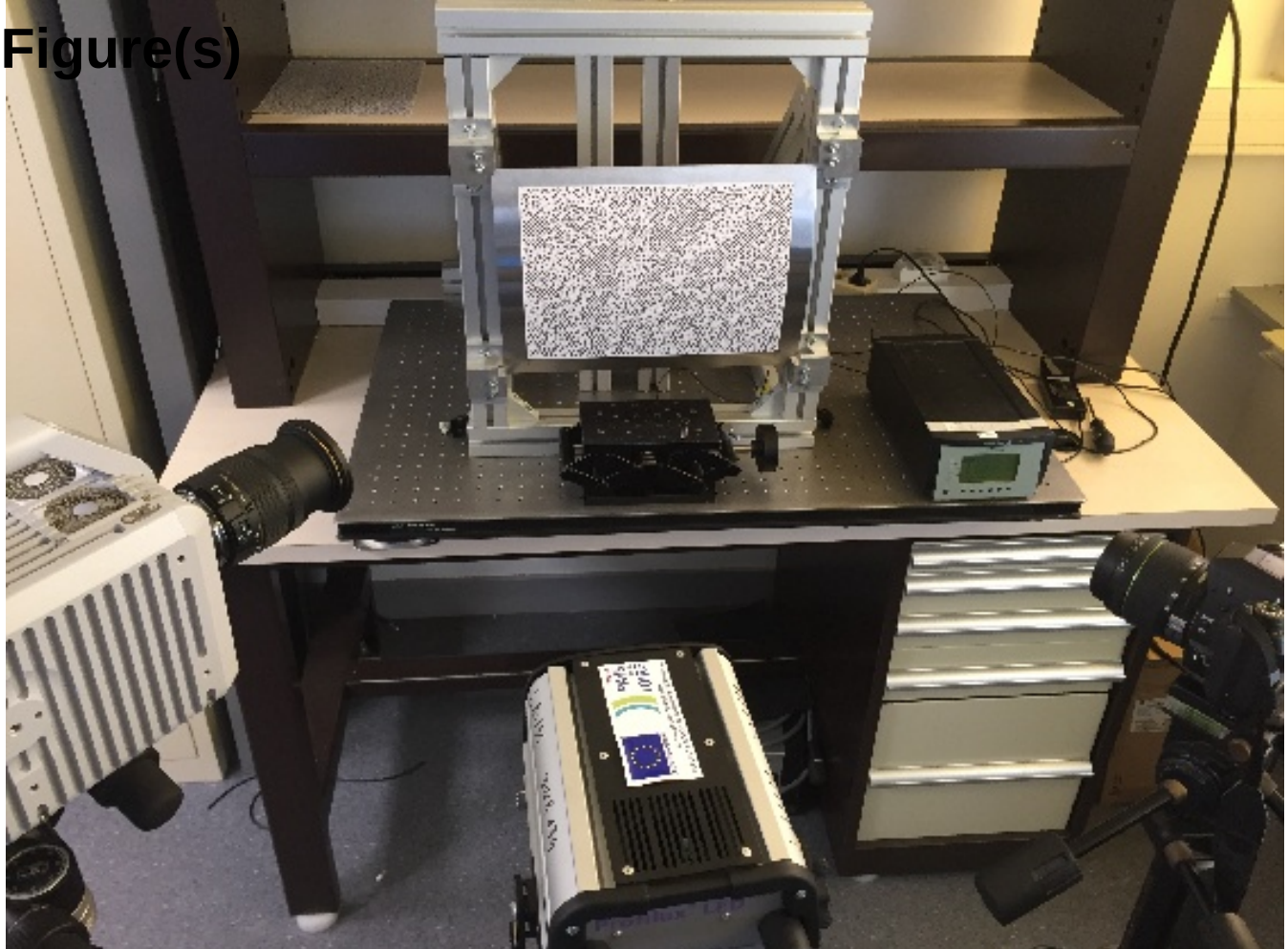

(a)

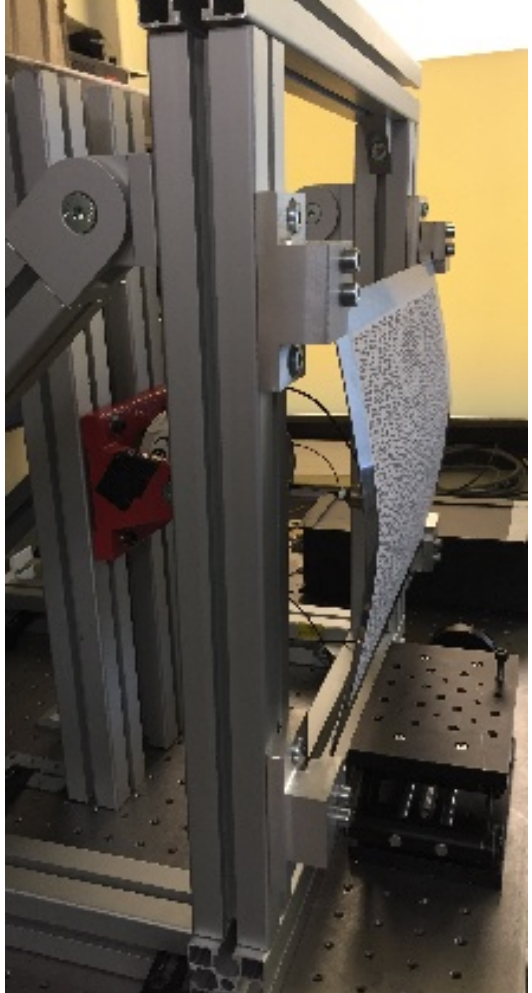

(b)

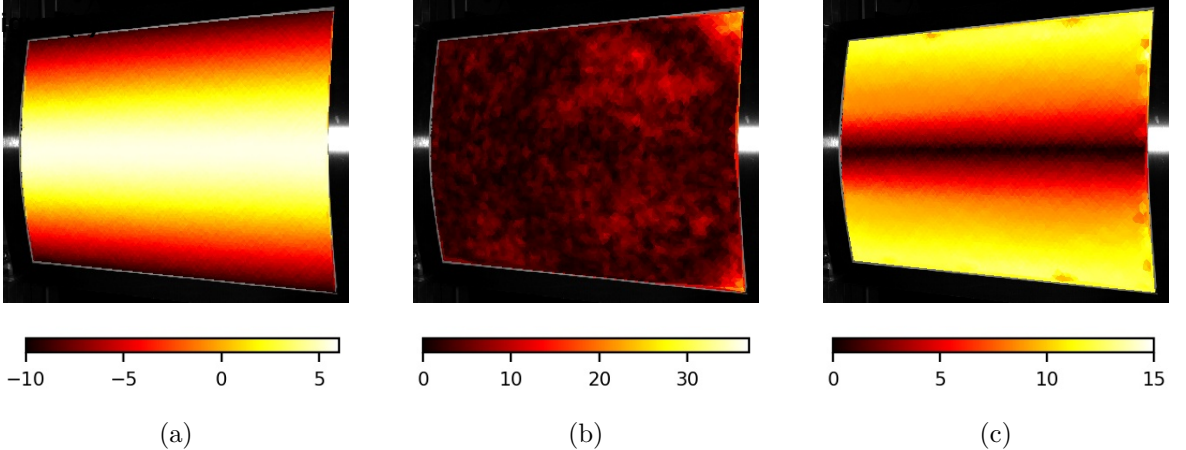


(a) (b) (c)

Figure

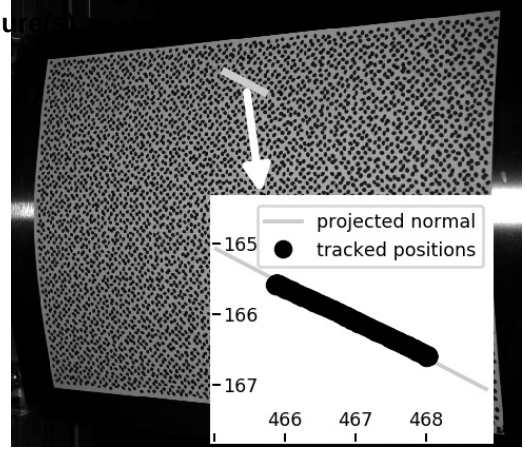
projected normal
tracked positions
165
166
167
466
467
468

(a)

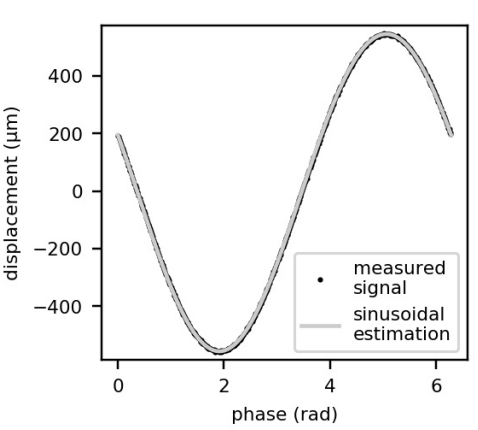
displacement (µm)
400
200
0
−200
−400
0
2
4
6
phase (rad)
measured signal
sinusoidal estimation

(b)

**Figure(s)**

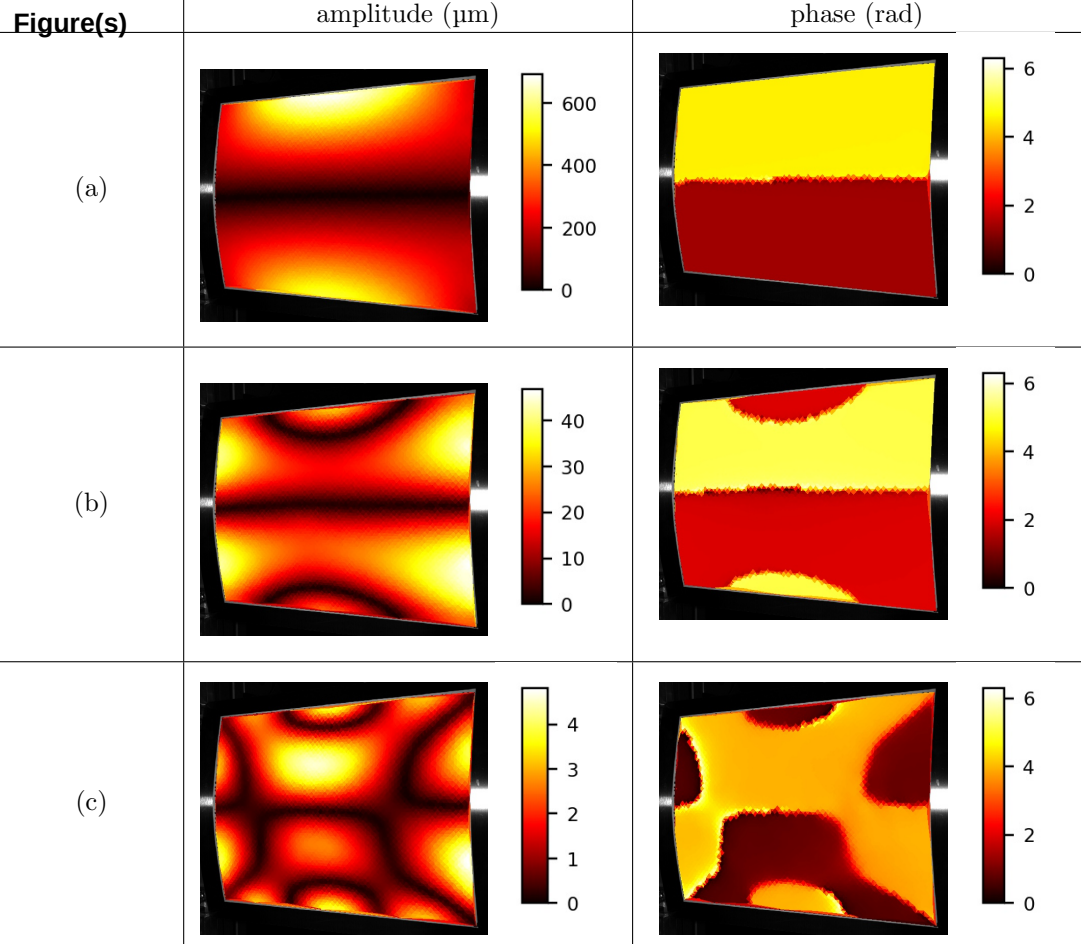
amplitude (μm)
phase (rad)
(a)
600
400
200
0
6
4
2
0
(b)
40
30
20
10
0
6
4
2
0
(c)
4
3
2
1
0
6
4
2
0

***Detailed Response to Reviewers**

Dear Ricardo Musafir

The authors gratefully thank the subject editor for its comments about their manuscript. We considered all remarks and made the required modifications (see below).

The authors,

1. Abstract: 3 lines from end: insert "is" before validated;

"is" has been inserted.

2. Next line: A bent plate => a bent plate;

Modifications have been done.

3. Abstract in the Abstract Box: Please update this abstract, making it identical to the one in the paper (in the present form, "firstly" is incorrectly written).

The abstract in the abstract box is now identical to the one in the manuscript.

4. Fig. 4 should, at least, have a) and b) parts ("top" and "bottom" should not be used).

(a) and (b) have been added, ("top" and "bottom" are not used anymore.

5. The upper arrow above z (or other symbols) should not be used, in Fig. 4 or elsewhere (for vectors, use boldface, as required in the JSV Guide for Authors) . In fact, I think it would be fine to identify the z axis simply by the symbol used for the (scalar) z coordinate.

"z" symbol is now used in all the document.

6. In Fig 7, the subfigures should be identified by a), b), …. f)

(a) to (f) have been added.

7. Fig. 11 also should have a) and b) parts (do not use upper and lower)

(a) to (c) have been added, ("upper" and "lower" are not used anymore.

8. Fig. 15 should have a), b) and c) parts. The frequency identification should be placed in the caption

(a) to (c) have been added, the frequency identification is now be placed in the caption.

***Style Checklist**

Journal of Sound and Vibration

Author Checklist

Authors should complete the following checklist and submit with their revised manuscript.

Math notation follows requirements on Guide for Authors (GFA) see: ☑

https://www.elsevier.com/journals/journal-of-sound-and-vibration/0022-460X/guide-for-authors

Use Roman (normal upright) type for: Total differential operators (e.g. d in differential); i or j (square root of -1); exp or e (base of natural logarithms); Re or Im (real or imaginary part); log, ln, sin, cos, etc.; abbreviations such as c.c. (complex conjugate); multiletter symbols (e.g. TL for transmission loss); subscripts of two or more letters identifiable as words or word-abbreviations (e.g., Apipe, fmax) ☑

For more unusual functions, JSV follows Abramowitz and Stegun's book. More detail given in the GFA (see link above).

Unit symbols - These should be upright (e.g. kg, not *kg*). ☑

All authors are listed on the manuscript with correct affiliations, correct email address and are in correct order. ☑

Keywords present. ☑

Manuscript is not currently submitted to any other Journal. ☑

If submitting highlights please note that only six may be submitted and each one should be no longer than 85 characters in length. ☑

Novelty of paper has been clearly stated in the Introduction. ☑

References are presented as per GFA. ☑

References not produced in English language to have English translation in brackets. ☑

Figures and Tables and Equations are numbered in sequence correctly. (See GFA). ☑

Nomenclature (if required) appears on second page of submission. ☑

Acknowledgements should appear in a separate section just after the conclusions. ☑

All abbreviations, in both the abstract and main body of document, are defined once only, the first time they appear in the text. (N.B. The Abstract is treated as an independent text, where references are given in full and abbreviations and symbols, if used, are properly defined.) ☑

Figures – if there are multi-parts to a figures each part is labelled (a) (b) (c) etc. and the labels defined in the figure caption. ☑

Figures – Colour can be used for the on-line version. Figures are reproduced in black and white in the printed journal and must therefore be readable in both colour and black & white. (N.B. charges apply for production of colour figures in the printed journal) ☑

Appendices – should appear before the list of references and labelled A, B, C, (please see GFA for further information regarding equations, figures and tables in the appendices. ☑

Copyright – material reproduced from other publications (e.g. Tables, Figures), source is acknowledged. ☑

Statement of Author contribution complete (see GFA) ☑

***Declaration of Interest Statement**

**Declaration of interests**

☒ The authors declare that they have no known competing financial interests or personal relationships that could have appeared to influence the work reported in this paper.

☐The authors declare the following financial interests/personal relationships which may be considered as potential competing interests: